Amino Acids (2016) 48:821–831
DOI 10.1007/s00726-015-2130-y

ORIGINAL ARTICLE

# Evaluation of GX1 and RGD-GX1 peptides as new radiotracers for angiogenesis evaluation in experimental glioma models

**Érica Aparecida de Oliveira[1,6] · Bluma Linkowski Faintuch[1] · Roselaine Campos Targino[2] · Ana Maria Moro[2] · Raquel Chacon Ruiz Martinez[3] · Rosana Lima Pagano[3] · Erich Talamoni Fonoff[3,4] · Camila de Godoi Carneiro[5] · Alexandre Teles Garcez[5] · Daniele de Paula Faria[5] · Carlos Alberto Buchpiguel[5]**

Received: 22 October 2015 / Accepted: 4 November 2015 / Published online: 23 November 2015


**Abstract** Gliomas are the most common type among all central nervous system tumors. The aggressiveness of gliomas is correlated with the level of angiogenesis and is often associated with prognosis. The aim of this study is to evaluate the novel GX1 peptide and the heterodimer RGD-GX1 radiolabeled with technetium-99m, for angiogenesis detection in glioma models. Radiolabeling and radiochemical controls were assessed for both radioconjugates. In vitro binding studies in glioma tumor cells were performed, as well as biodistribution in *SCID* mice bearing tumor cells, in order to evaluate the biological behavior and tumor uptake of the radiocomplexes. Blocking and imaging studies were also conducted. MicroSPECT/CT images were acquired in animals with experimentally implanted intracranial tumor. Open field activity was performed to evaluate behavior, as well as perfusion and histology analysis. The radiochemical purity of both radiotracers was greater than 96 %. In vitro binding studies revealed rather similar binding profile for each molecule. The highest binding was for RGD-GX1 peptide at 120 min in U87MG cells (1.14 ± 0.35 %). Tumor uptake was also favorable for RGD-GX1 peptide in U87MG cells, reaching 2.96 ± 0.70 % at 1 h p.i. with 47 % of blocking. Imaging studies also indicated better visualization for RGD-GX1 peptide in U87MG cells. Behavior evaluation pointed brain damage and histology studies confirmed actual tumor in the uptake site. The results with the angiogenesis seeking molecule $^{99m}$Tc-HYNIC-E-[c(RGDfk)-c(GX1)] were successful, and better than with $^{99m}$Tc-HYNIC-PEG$_4$-c(GX1). Future studies targeting angiogenesis in other glioma and nonglioma tumor models are recommended.

**Keywords** RGD peptide · GX1 peptide · Technetium-99m · Angiogenesis · Glioma · Tumor

✉ Érica Aparecida de Oliveira
ericaoliveira@usp.br

1 Radiopharmacy Center, Institute of Energy and Nuclear Research, Av. Prof. Lineu Prestes, 2242, São Paulo 05508-000, Brazil

2 Laboratory of Biopharmacology in Animal Cells, Butantan Institute, Av. Vital Brasil, 1500, Sao Paulo 05503-900, Brazil

3 Laboratory of Neuromodulation and Experimental Pain, Teaching and Research Institute, Hospital Sírio-Libanês, Rua Professor Daher Cutait, 69, Sao Paulo 01308-060, Brazil

4 Division of Functional Neurosurgery, Institute of Psychiatry of Hospital das Clinicas and Department of Neurology, School of Medicine, University of São Paulo, R. Dr. Ovídio Pires de Campos, 785, São Paulo 01060-970, Brazil

5 Nuclear Medicine Laboratory (LIM 43), Medical School, University of São Paulo, Av. Dr. Enéas de Carvalho Aguiar, s/nº-Rua 1, Sao Paulo 05403-900, Brazil

6 Present Address: School of Pharmaceutical Sciences, University of Sao Paulo, Av. Prof. Lineu Prestes, 580 Bloco 17, São Paulo 05508-900, Brazil

## Introduction

Peptides have great importance in receptor targeting of tumors, due to some optimal features when compared to other targeting agents like monoclonal antibodies and their derivatives (Durkan et al. 2007; Okarvi 2004; Oyen et al. 2007; Song et al. 2012). Many types of peptides have been studied, and several cancer cells were found to express peptide receptors (Achilefu 2004; Reubi 1997; Reubi et al. 2005). The phage display peptide library is useful for identifying specific peptide sequences for known receptors (Ueberberg and Schneider 2010).

Gliomas, particularly glioblastoma multiforme, are the most common type among all central nervous system tumors. Usually, patients have a poor prognosis (Hua et al. 2014). Surgery and radiotherapy can be effective; however, indication may be limited due to various factors, including the close proximity of the tumor to important functional cerebral regions (Ong et al. 2009). The mean survival of patients with glioblastoma multiforme is 35 % after 1 year, and less than 5 % of patients survive more than 5 years (Ostrom et al. 2013).

A very promising biological target in this context is tumor-induced angiogenesis. Newly formed blood vessels show high expression of specific molecules, which are absent in mature vasculature (Pasqualini et al. 2002). Angiogenesis plays a critical role in glioma development and growth, even during the earliest phases. It is permissive for metastasis and represents a pathological hallmark of this cancer. The level of angiogenesis correlates with the aggressiveness of gliomas, and is often associated with prognosis (Bello et al. 2004; Skobe et al. 1997).

An example of angiogenesis target is $\alpha_v\beta_3$ integrin receptor, which is strongly overexpressed on the activated endothelium of new blood vessels (Strijkers et al. 2010). The $\alpha_v\beta_3$ integrins are attached to extracellular matrix proteins, and recognize the sequence arginine-glycine-aspartic acid (RGD) as a potential binding site (Ruoslahti and Pierschbacher 1986).

The motif RGD (Arg-Gly-Asp) is a cell recognition and attachment site for a number of extracellular matrix proteins as well as blood and cell surface proteins, and has important regulatory functions in many biological activities. RGD is involved in cell attachment, cell spreading, actin-skeleton formation, and focal-adhesion formation with integrins; for these reasons it is widely used for cancer targeting (Desgrosellier and Cheresh 2010; Guo and Giancotti 2004; Hynes 1992; Jin et al. 2010; Koivunen et al. 1995; Pasqualini et al. 1997; Wu et al. 2014). The GX1 peptide is a novel vascular marker for human cancers, and recent studies suggest integrin α3β1 as a possible receptor, although there is still a lack in the understanding the mechanism of GX1 (Hu et al. 2014; Hui et al. 2008; Zhi et al. 2004).

A heterodimer molecule consisting by RGD and GX1 motif in one probe, both in a cyclic conformation, is an attractive approach, because many cancer types simultaneously express multiple receptors, increasing the molecular target. Peptide heterodimers have shown especially good performance for in vivo cancer imaging. The success of these molecular probes demonstrates that the dual-targeting strategy is generally a good approach for developing molecular probes. This approach has been used in many studies with successful results as reported in Liu and Wang (2010) review.

Preliminary studies showed great advantages of these molecules with regard to radiolabeling features and biodistribution in vivo (Oliveira and Faintuch 2015). They were also preliminarily conjugated to magneto nanoparticles in our experience, and visualized by MRI, for confirmation of their specificity in glioma tumor cells (Oliveira, unpublished results).

The aim of this study was to investigate the receptor-targeting and tumor diagnostic value for glioma, of the novel GX1 peptide alone, as well as combined in the form of RGD-GX1 heterodimeric peptide, both labeled with technetium-99m, using the specific target of these peptides in vascular and tumor tissue to promote a novel tool for detecting this tumor in early stages.

## Methods

### Radiolabeling

Preparation and labeling procedures for HYNIC-$PEG_4$-c(GX1) and HYNIC-E-[c(RGDfk)-c(GX1)] peptides (CPC Scientific Inc., CA, USA) were recently reported by our group (Oliveira and Faintuch 2015). In brief, it was added to a sealed reaction vial 20 mg of tricine and 5 mg of EDDA (ethylenediamine-*N*,*N*′-diacetic acid) dissolved in phosphate buffer 0,1 N, 10 μL of the respective peptide (μg/mL), stannous chloride in HCl solution 0.1 M, and 500 μL of $Na^{99m}TcO_4$ (1850 MBq) ($^{99}Mo/^{99m}Tc$ generator from Institute of Energy and Nuclear Research, Sao Paulo, SP, Brazil). Reaction was induced by heating at 100 °C for 20 min. All reagents were acquired from Merck and Sigma–Aldrich (Sao Paulo, Brazil). The radiochemical evaluation was assessed by Instant Thin Layer Chromatography (ITLC) and confirmed by reverse phase high performance liquid chromatography (RP-HPLC, Shimadzu, Kyoto, Japan) using a C18 column (5.0 mm, 100 A°, 4.6 × 250 mm, Waters, Milford, MA) and a flow rate of 1.0 mL/min.

### Cell culture

Tumor cell lines of human glioblastoma U87MG and T98G (American Type Culture Collection, USA) were grown in DMEM (Dulbecco's modified Eagle's Medium) and Ham's F12 Nutrient Mixture medium, supplemented with 10 % (v/v) fetal calf serum (Sigma-Aldrich, USA). Cells were kept in a humidified air environment containing 5 % $CO_2$ at 37 °C. They were grown to almost confluence and then harvested by trypsinization. The cells were tested for misidentification and/or cross-contamination.

Tumor cells ($10^6$ cells/well) were seeded into well culture plates for the binding studies 24 h before the

experiment. Studies were performed in triplicate ($n = 3$). Cells for inoculation in animals were centrifuged (5 min at $100\times g$), counted, and then resuspended in PBS for administration in the animals.

### In vitro cell binding assay

Cells were rinsed with an ice-cold assay medium, followed by addition of the assay medium and the radiotracers $^{99m}$Tc-HYNIC-PEG$_4$-c(GX1) or $^{99m}$Tc-HYNIC-E-[c(RGDfk)-c(GX1)] to the cultured wells (5.55 mBq/well). For nonspecific binding assays, cold conjugate (1 mmol/L/well) was added. After incubation at 37 °C for 5, 30, 60, 90, and 120 min, cells were rinsed twice with PBS. Cell surface-bound radioligand was removed by acid wash (50 mmol/L of glycine and 1 mol/L of NaCl, pH = 2.8) at room temperature for 5 min. The cells were lysed with NaOH (1 N) to determine the amount of internalized radioligand. All phases were collected in measurement tubes for counting.

### Biodistribution studies

U87MG or T98G tumor cells ($5 \times 10^6$ in 0.1 mL) were subcutaneously inoculated on the right flank of *SCID* (severe combined immunodeficiency) mice (20–25 g). When tumors reached approximately 1 cm diameter, biodistribution of $^{99m}$Tc-HYNIC-PEG$_4$-c(GX1) and $^{99m}$Tc-HYNIC-E-[c(RGDfk)-c(GX1)] was conducted at 1 h post injection (p.i.) for both radiotracers and at 2 h p.i. for the heterodimer radiotracer. Animals were injected with the radiolabeled complex (18.5 MBq/0.05 mL) via the tail vein. Specific uptake studies were also conducted by co-injecting an excess (50 μL, 1 mg/mL) of unlabeled peptide for receptor blocking.

All urethane-anesthetized animals ($n = 5$) were sacrificed by cervical dislocation and organs and tissues of interest were harvested, weighed and counted. The radioactivity in each organ was expressed as a percentage of the injected dose per gram of organ (%ID/g).

Experiments were carried out in compliance with the guidelines for animal experimentation, Scientific Ethics Committee, IPEN/CNEN-SP.

### Intracranial surgery

Animals (athymic *nude* rats NIH-WHn, 200–300 g) were anesthetized with a mixture of Ketamine, Xylazine and Morfin and fixed in a stereotaxic frame (David Kopf, Tujunga, CA). The upper incisor bar was set at 3.3 mm below the interaural line, such that the skull was horizontal between bregma and lambda. Each animal received two stereotaxic injection that were aimed to striatum using bregma as the reference for each plane antero-posterior (AP) = 0.0 mm Mm; medio-lateral (ML) = 3 mm and dorso-ventral (DV) = 4,5 mm. A total of 5 μl of the U87MG cells was unilaterally implanted by stereotaxic injection, at the rate of 1.0 μl per min (80,000 cells/μL). A second injection followed in the opposite hemisphere of the brain containing DMEM medium as control.

Neurological signs such as seizures, weakness, unsteady gait, excessive circling behavior or marked aggression or timidity, along with signs of pain or discomfort, were considered as indicators of tumor mass.

### Scintigraphic imaging

Scintigraphy was performed in a planar single-headed scanner (Mediso Imaging System, Budapest, Hungary), equipped with a low-energy, high-resolution collimator. The system was calibrated for technetium-99m with a 20 % energy window set at 140 keV, using a 256 × 256 × 16 matrix size. Semiquantification of the tumor uptake was determined by using region-of-interest (ROI) analysis, using the following equation:

$$\%\ \text{tumor activity} = (\text{tumor cpm} \times 100)/(\text{injected dose in cpm} - \text{background cpm}).$$

### Small animal SPECT/CT imaging

This study was performed just as a proof of concept, due to the superiority of $^{99m}$Tc-HYNIC-E-[c(RGDfk)-c(GX1)] at U87MG cells found in the previous analysis of in vitro binding and tumor biodistribution.

For small animal SPECT/CT imaging (Triumph Trimodality-Gamma Medica Ideas, California, USA), the animal ($n = 1$) was anesthetized with 3 % isoflurane in 100 % oxygen and injected in the penile vein with 33 MBq of $^{99m}$Tc-HYNIC-E-[c(RGDfk)-c(GX1)] in 0.1 mL.

SPECT images (32 projections of 60 s per detector) were obtained 60 min after tracer injection using a dual-head camera with 1.0 mm five-pinhole collimators and CZT detector system. Images were reconstructed using OSEM method. CT images were acquired immediately before SPECT imaging for helping the best positioning of the animal´s brain at the center of the field of view (FOV) and anatomical information for fusion with SPECT images. Images were acquired using a flat panel detector CT system with 45 kVp and 390 μA. Images (SPECT and CT) were fused using PMOD™ software.

### Open-field activity

This study was performed with six rats including one control rat without surgery, and two animals with intracranial tumor. Each rat was placed in the center of the

open-field (40 × 40 × 60 cm) and allowed to freely explore for 5 min. After each animal, the open field was cleaned with 5 % ethanol and then dried with a dry cloth. The sessions were recorded with a video camera and displacements and behavior were recorded using X-Plot Rat (X-Plot Rat Program 2005 Beta 1.0.1. It was evaluated for total entries, total distance, and frequency and time spent of rearing (partial or total raising on the hind limbs).

### Perfusion and histology analysis

Animals with intracranial tumor were anesthetized with thiopental (40 mg/kg) and perfused transcardially with 4 % paraformaldehyde in 0.1 M phosphate buffer (pH 7.4). Brains were removed, bathed in 4 % paraformaldehyde for 3 h, and then transferred to a 20 % sucrose/0.1 M phosphate buffer solution at 4 °C overnight. Frozen sections (40 µm) were then cut with a sliding microtome along the frontal plane and Nissl staining was used.

### Statistical analysis

All data were expressed as mean ± standard deviation (SD). Student's *t* test was used for comparisons and $p < 0.05$ was considered statistically significant. Also the data were analyzed using a one-way analysis of variance. Significant differences in the means were determined using multiple comparisons with the Tukey–Kramer test at a significance level of $p < 0.05$.

## Results

Radiochemical purity of $^{99m}$Tc-HYNIC-PEG$_4$-c(GX1) and $^{99m}$Tc-HYNIC-E-[c(RGDfk)-c(GX1)] was higher than 96 % for both conjugates with single peak for each in HPLC analysis, as established in Oliveira and Faintuch (2015).

In vitro studies with glioma tumor cell achieved very similar binding profile for each radiotracer (Fig. 1). Total binding of $^{99m}$Tc-HYNIC-PEG$_4$-c(GX1) had a peak at 60 min of incubation for U87MG and T98G cells, with values of 0.69 ± 0.06 and 0.54 ± 0.05 % ($p < 0.05$), respectively. For U87MG, specific binding was around 20 % of total binding and total internalization 7 %. Additionally, for T98G, these values were 35 and 3 %, respectively.

$^{99m}$Tc-HYNIC-E-[c(RGDfk)-c(GX1)] had higher total binding values at 120 min of incubation for both cells, especially for U87MG which achieved 1.14 ± 0.35 %, while for T98G was 0.45 ± 0.03 % ($p < 0.05$). Yet, U87MG cells also had a remarkable specific binding of 75 %, whilst T98G had low uptakes.

The results of the biodistribution studies in U87MG and T98G cells are summarized in Table 1. Values are expressed as % of injected dose/gram (for blood %ID/mL). The biodistribution revealed predominant renal excretion with a percentage remained in intestinal tract for both radiotracers, blood uptake in the range of 1 %ID/mL at 1 h p.i. and lower at 2 h p.i., and uptake in most organs and tissues around 2 %ID/g. The 1 and 2 h time adopted for biodistribution imaging were based on blood clearance of the radiotracer in a previous study using *Balb/c* mice (Oliveira and Faintuch 2015) and from in vitro results in this work.

Tumor uptake was more pronounced in animals bearing U87MG tumor cells. At 1 h, the $^{99m}$Tc-HYNIC-E-[c(RGDfk)-c(GX1)] radiotracer obtained tumor uptake of 2.96 ± 0.70 %ID/g, while $^{9m}$Tc-HYNIC-PEG$_4$-c(GX1) achieved 1.52 ± 0.34 %ID/g ($p < 0.005$). The co-administration of an excess amount of unlabeled peptide decreased the uptake of $^{99m}$Tc-HYNIC-PEG$_4$-c(GX1) and $^{99m}$Tc-HYNIC-E-[c(RGDfk)-c(GX1)] for around 47 % (Table 1; Fig. 2).

At 2 h, the uptake was 2.87 ± 0.53 %ID/g for RGD-GX1 peptide with almost 69 % of blocking, however this uptake had no significant difference when compared to 1 h ($p > 0.5$).

Biodistribution results showed a remarkable uptake in mice bearing T98G tumor cells at 60 min with $^{99m}$Tc-HYNIC-E-[c(RGDfk)-c(GX1)] radiotracer (2.49 ± 0.30 %ID/g), when compared to $^{99m}$Tc-HYNIC-PEG$_4$-c(GX1) (0.78 ± 0.44 %ID/g), ($p < 0.001$). The tumor was 42 % blocked by GX1 cold peptide and 46 % by RGD-GX1 cold peptide (Table 1; Fig. 2). At 120 min the tumor uptake was 1.58 ± 0.60 %ID/g for $^{99m}$Tc-HYNIC-E-[c(RGDfk)-c(GX1)] and 50 % was blocked, even so with no significant difference when compared to 1 h ($p > 0.5$).

The tumor/muscle ratio was highest in animals bearing glioma tumor cells (U87MG), reaching 2.55 for GX1 radiotracer and for RGD-GX1 peptide 5.83 and 3.29 for 1 and 2 h, respectively. With T98G cells the highest ratio was for tumor/blood (2.7) and tumor/muscle ratio (4.8) (Fig. 2).

Best visualization was documented for U87MG tumor at 1 h employing $^{99m}$Tc-HYNIC-E-[c(RGDfk)-c(GX1)], with ROI value of 8.72 %, and 0.78 % for blocking (Fig. 3). $^{99m}$Tc-HYNIC-PEG$_4$-c(GX1) had a lower uptake, however also permitted good imaging, with ROI of 5.21 %, and 1.66 % for blocking.

At 2 h, the intensity of U87MG tumor uptake decreased in the imaging with $^{99m}$Tc-HYNIC-E-[c(RGDfk)-c(GX1)] (ROI of 3.87 and 0.65 % for blocking), thus rendering the 1 h time point as the best for imaging acquisition.

Images of T98G tumor cells with both radiotracers are shown at Fig. 3. $^{99m}$Tc-HYNIC-PEG$_4$-c(GX1) achieved ROI of 1.21 and 0.34 % for blocking at 1 h p.i., whereas for $^{99m}$Tc-HYNIC-E-[c(RGDfk)-c(GX1)] the results were

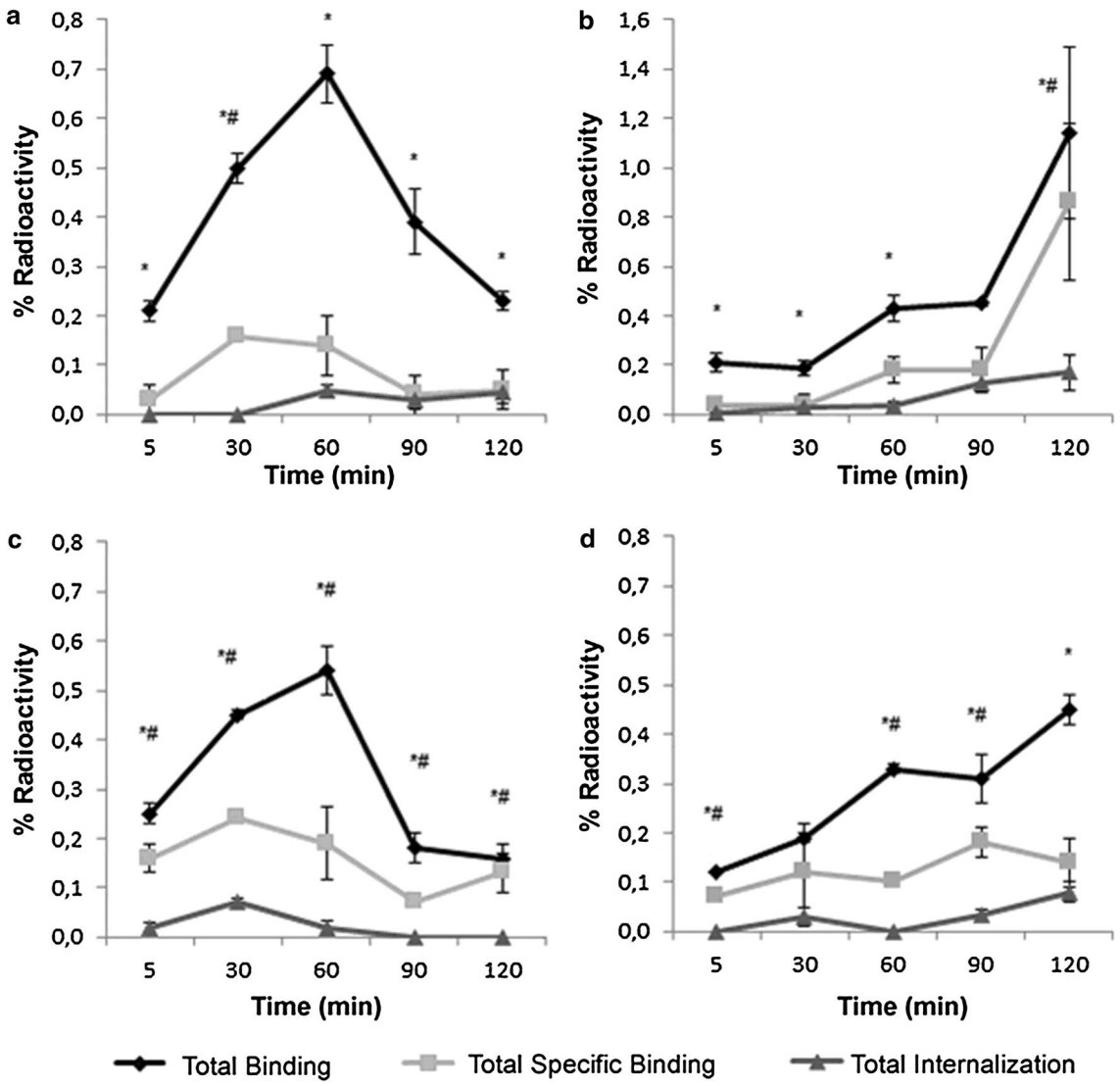


**Fig. 1** Uptake binding in U87MG human glioma cells **a** $^{99m}$Tc-HYNIC-PEG$_4$-c(GX1); **b** $^{99m}$Tc- HYNIC-E-[c(RGDfk)-c(GX1)]; and in T98G glioma cells; **c** $^{99m}$Tc-HYNIC-PEG$_4$-c(GX1); **d** $^{99m}$Tc-HYNIC-E-[c(RGDfk)-c(GX1)]. Significances are indicated *total binding vs total specific binding and total internalization; #total specific binding vs total internalization

2.63 and 0.33 %, respectively. At 2 h $^{99m}$Tc-HYNIC-E-[c(RGDfk)-c(GX1)] showed best visualization, with ROI of 3.18 and 0.38 % for blocking.

Although these values are lower than those corresponding to U87MG cells, the pattern is sustained, with higher uptake from the heterodimer peptide at 1 h.

Small animal SPECT/CT images enabled the tumor visualization in the region of left striatum (right in the images), nevertheless with little uptake difference, when compared to adjacent tissues. Still, uptake was clear when compared to the opposite side (left side in the image). Two out of ten animals bearing tumors located at motor cortex ($n = 1$) and striatum ($n = 1$) are depicted in Fig. 4. Data presented at Fig. 5 revealed a tendency for decreasing exploratory activity, when tumor was located at the motor cortex.

## Discussion

Brain tumors represent a difficult challenge for patients and physicians. Usually located in hard-to-reach areas, they may be resistant to radiation and chemotherapy. Surgery is not always feasible, and there is some risk of brain dysfunctions and other sequelae. Nowadays, most of the drugs used for cancer cannot fully differentiate between healthy cells and malignant ones, leading to some degree of systemic toxicity and additional side effects (Gautam et al. 2014).

The need for new diagnostic methods for glioma, and the fact that it induces angiogenesis as one of its main biological and molecular features, stimulates new experimental studies. Short peptide sequences with affinity for new

**Table 1** Biodistribution of $^{99m}$Tc-HYNIC-PEG$_4$-c(GX1) and $^{99m}$Tc-HYNIC-E-[c(RGDfk)-c(GX1)] in *SCID* mice bearing U87MG and T98G human glioblastoma cell line at 60 and 120 min p.i. ($n = 5$)

| Organ/tissue (%ID/g ± SD) | GX1 | GX1 block | RGD-GX1 | RGD-GX1 block | RGD-GX1 | RGD-GX1 block |
|---|---|---|---|---|---|---|
| Time | 1 h | | | | 2 h | |
| *U87MG cells* | | | | | | |
| Blood | 1.22 ± 0.34 | 1.27 ± 1.16 | 1.20 ± 0.11 | 1.09 ± 0.18 | 0.78 ± 0.11 | 0.59 ± 0.07 |
| Heart | 1.38 ± 0.30 | 0.55 ± 0.23 | 1.10 ± 0.27 | 0.93 ± 0.53 | 1.72 ± 0.43 | 1.51 ± 0.40 |
| Lungs | 2.23 ± 0.70 | 1.34 ± 0.63 | 2.48 ± 0.67 | 1.86 ± 0.87 | 3.88 ± 0.54 | 3.38 ± 0.47 |
| Kidneys | 22.31 ± 8.19 | 14.97 ± 1.68 | 46.87 ± 15.45 | 28.68 ± 9.22 | 16.95 ± 4.88 | 13.98 ± 1.61 |
| Spleen | 1.05 ± 0.50 | 0.46 ± 0.35 | 3.29 ± 1.45 | 1.54 ± 0.92 | 3.25 ± 0.41 | 2.79 ± 0.40 |
| Stomach | 1.62 ± 0.68 | 1.17 ± 0.26 | 3.61 ± 0.80 | 1.54 ± 0.01 | 3.23 ± 0.56 | 1.34 ± 0.12 |
| Pancreas | 2.31 ± 0.79 | 0.81 ± 0.43 | 1.54 ± 0.45 | 1.07 ± 0.62 | 2.34 ± 0.52 | 2.33 ± 0.82 |
| Liver | 2.33 ± 0.69 | 2.26 ± 1.27 | 2.61 ± 0.61 | 0.94 ± 0.11 | 6.83 ± 0.86 | 6.17 ± 1.97 |
| Large intestine | 2.39 ± 0.99 | 0.77 ± 0.22 | 4.27 ± 0.39 | 1.83 ± 0.70 | 4.15 ± 1.66 | 2.29 ± 0.56 |
| Small intestine | 1.85 ± 0.34 | 0.95 ± 0.56 | 8.87 ± 1.74 | 1.96 ± 0.65 | 3.85 ± 0.74 | 3.50 ± 1.00 |
| Muscle | 0.59 ± 0.25 | 0.40 ± 0.15 | 0.51 ± 0.21 | 0.40 ± 0.26 | 0.87 ± 0.23 | 0.84 ± 0.73 |
| Bone | 1.55 ± 0.25 | 1.04 ± 0.38 | 1.47 ± 0.51 | 1.15 ± 0.73 | 2.11 ± 0.17 | 2.01 ± 0.34 |
| Brain | 0.21 ± 0.11 | 0.11 ± 0.04 | 0.16 ± 0.04 | 0.13 ± 0.08 | 0.25 ± 0.05 | 0.24 ± 0.08 |
| Tumor | 1.52 ± 0.34 | 0.72 ± 0.34 | 2.96 ± 0.70 | 1.40 ± 0.30 | 2.87 ± 0.53 | 1.98 ± 0.18 |
| *T98G cells* | | | | | | |
| Blood | 1.83 ± 1.06 | 1.19 ± 0.37 | 1.57 ± 0.79 | 1.11 ± 0.37 | 0.58 ± 0.32 | 0.38 ± 0.28 |
| Heart | 0.57 ± 0.25 | 0.25 ± 0.07 | 1.21 ± 0.53 | 1.04 ± 0.58 | 0.43 ± 0.14 | 0.17 ± 0.06 |
| Lungs | 1.22 ± 0.55 | 0.57 ± 0.12 | 2.51 ± 0.56 | 2.26 ± 0.93 | 1.06 ± 0.26 | 0.48 ± 0.10 |
| Kidneys | 14.57 ± 5.37 | 10.96 ± 3.42 | 26.50 ± 8.74 | 21.88 ± 6.58 | 21.55 ± 4.40 | 21.52 ± 9.32 |
| Spleen | 0.57 ± 0.34 | 0.27 ± 0.05 | 2.26 ± 0.21 | 1.55 ± 0.67 | 1.44 ± 0.53 | 0.66 ± 0.23 |
| Stomach | 1.81 ± 0.30 | 2.07 ± 0.60 | 1.80 ± 0.76 | 1.90 ± 0.89 | 2.46 ± 0.34 | 1.72 ± 0.46 |
| Pancreas | 0.70 ± 0.39 | 0.28 ± 0.06 | 1.21 ± 0.57 | 1.26 ± 0.57 | 0.55 ± 0.07 | 0.22 ± 0.09 |
| Liver | 1.38 ± 1.23 | 0.49 ± 0.03 | 3.31 ± 1.05 | 3.66 ± 0.20 | 1.44 ± 0.78 | 0.82 ± 0.59 |
| Large intestine | 0.90 ± 0.57 | 0.97 ± 0.49 | 3.21 ± 0.89 | 1.78 ± 1.28 | 2.02 ± 0.41 | 0.70 ± 0.26 |
| Small intestine | 1.15 ± 0.85 | 1.07 ± 0.70 | 4.97 ± 0.74 | 1.57 ± 0.35 | 3.70 ± 0.58 | 1.01 ± 0.15 |
| Muscle | 0.28 ± 0.08 | 0.23 ± 0.06 | 0.63 ± 0.21 | 0.52 ± 0.02 | 0.33 ± 0.24 | 0.06 ± 0.01 |
| Bone | 0.81 ± 0.44 | 0.53 ± 0.32 | 1.17 ± 0.38 | 1.40 ± 0.15 | 0.57 ± 0.11 | 0.48 ± 0.27 |
| Brain | 0.10 ± 0.07 | 0.05 ± 0.03 | 0.15 ± 0.04 | 0.12 ± 0.07 | 0.07 ± 0.03 | 0.03 ± 0.01 |
| Tumor | 0.78 ± 0.44 | 0.45 ± 0.16 | 2.49 ± 0.30 | 1.33 ± 0.29 | 1.58 ± 0.60 | 0.79 ± 0.37 |

blood vessels and tumor cells represent suitable molecular probes for imaging in a non-invasive way, leading to a more effective diagnostic approach.

Preliminary evaluations of the peptide sequences GX1 and RGD-GX1 by our group, demonstrated advantageous properties for such diagnostic radiopharmaceuticals when radiolabeled with technetium-99m (Oliveira and Faintuch 2015), along with high specificity in U87MG glioblastoma tumor cells, when conjugated to magnetonanoparticles (Oliveira, unpublished results).

The binding studies pointed out very similar profiles for both radiotracers in all cell lines studied. The total binding in HUVEC cells was lower than in tumor cells, suggesting specificity only for glioblastoma cells (Oliveira and Faintuch 2015). In fact, this was just a portion of the potential binding, since the main target is the new vasculature that may solely be reproduced in vivo.

Chen et al. (2012) studied the GX1 molecule radiolabeled with $^{64}$Cu in animals bearing U87MG tumor cells, with tumor uptake of 6.46 ± 0.29 %ID/g at 24 h p.i. At in vitro assays, the maximum binding value was 0.29 % at 2 h, among all radioactivity inputs. The total binding achieved in the present study, with $^{99m}$Tc-HYNIC-E-[c(RGDfk)-c(GX1)] in the same cell model, contrasts with their conclusion.

$^{99m}$Tc-HYNIC-E-[c(RGDfk)-c(GX1)] exhibited best results in binding assays at 2 h, and U87MG cells achieved the highest values, standing out from others. Biodistribution in mice bearing tumors from the same cells, indicated high uptakes for this radiotracer, confirming the results of in vitro studies. The tumor can be well visualized in all

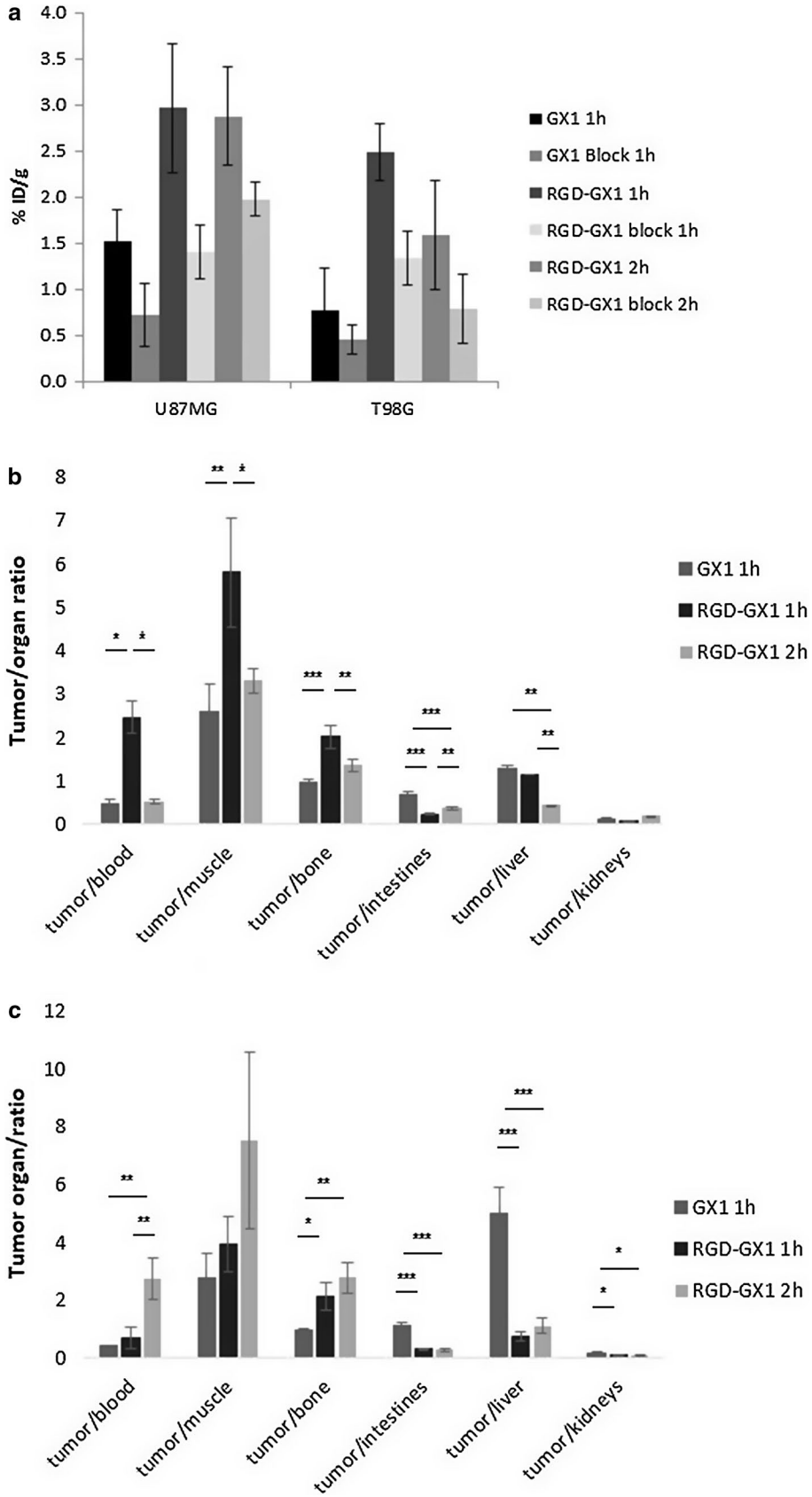


**Fig. 2** Uptake of radiotracers **a** $^{99m}$Tc-HYNIC-PEG$_4$-c(GX1) and $^{99m}$Tc- HYNIC-E-[c(RGDfk)-c(GX1)] in tumor and blocked tumor of *SCID* mice bearing U87MG or T98G cells, 1 and 2 h after injection; **b**, **c** Tumor/organ and tumor/tissue ratios of $^{99m}$Tc-HYNIC-PEG$_4$-c(GX1) and $^{99m}$Tc-HYNIC-E-[c(RGDfk)-c(GX1)] **b** in U87MG cells; **c** in T98G cells. Significances are indicated by $***p < 0.001$, $**p < 0.01$, $*p < 0.5$

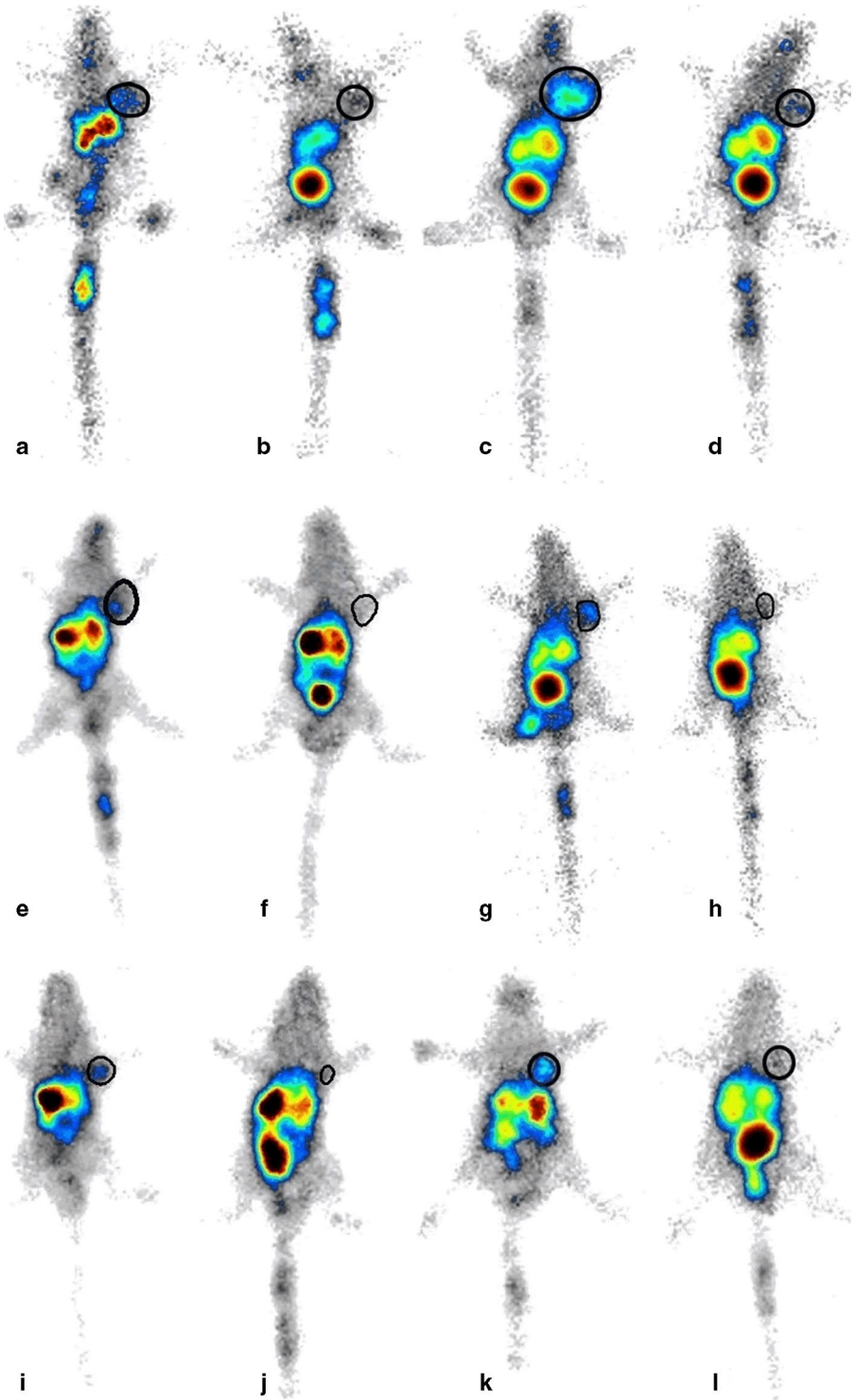


**Fig. 3** Scintigraphic image in urethane-anesthetized **a–f** *SCID* mice bearing U87MG glioma tumor at 1 h p.i. **a** $^{99m}$Tc-HYNIC-PEG$_4$-c(GX1); **b** $^{99m}$Tc-HYNIC-PEG$_4$-c(GX1) block; **c** $^{99m}$Tc-HYNIC-E-[c(RGDfk)-c(GX1)]; **d** $^{99m}$Tc-HYNIC-E-[c(RGDfk)-c(GX1)] block; at 2 h p.i. **e** $^{99m}$Tc-HYNIC-E-[c(RGDfk)-c(GX1)]; **f** $^{99m}$Tc-HYNIC-E-[c(RGDfk)-c(GX1)] block; **g–l** *SCID* mice bearing T98G glioma tumor at 1 h p.i. **g** $^{99m}$Tc-HYNIC-PEG$_4$-c(GX1); **h** $^{99m}$Tc-HYNIC-PEG$_4$-c(GX1) block; **i** $^{99m}$Tc-HYNIC-E-[c(RGDfk)-c(GX1)]; **j** $^{99m}$Tc- HYNIC-E-[c(RGDfk)-c(GX1)] block; at 2 h p.i. **k** $^{99m}$Tc-HYNIC-E-[c(RGDfk)-c(GX1)]; **l** $^{99m}$Tc-HYNIC-E-[c(RGDfk)-c(GX1)] block (0.05 mL/18,5 MBq)

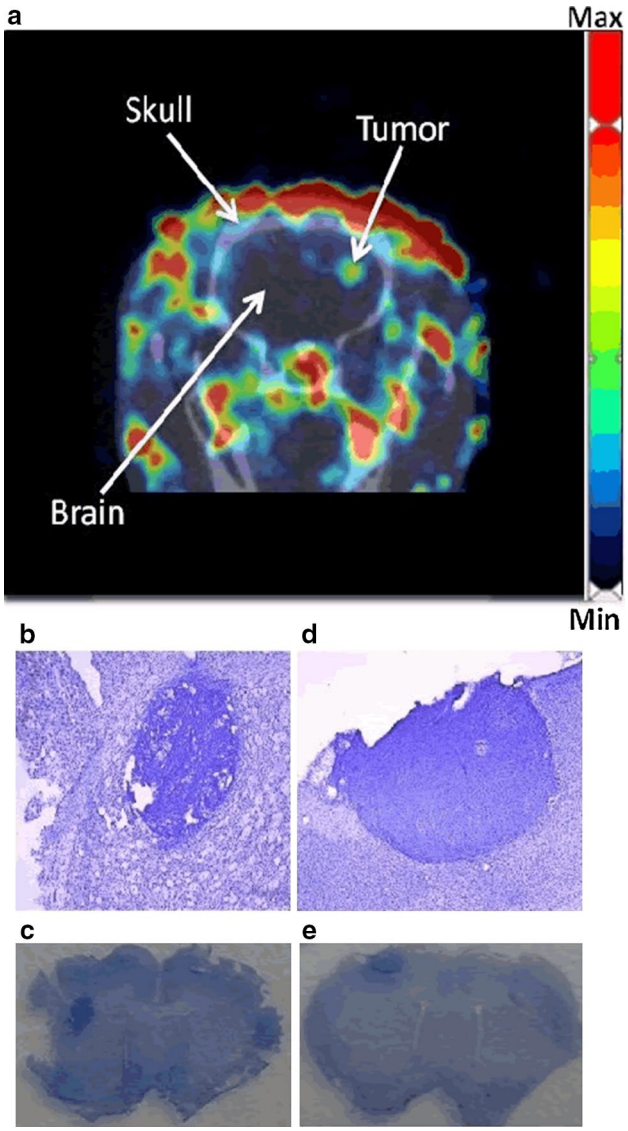


**Fig. 4** **a** Illustrative SPECT/CT image (*coronal view*) of nude rat bearing U87MG glioma intracranial obtained with $^{99m}$Tc-HYNIC-E-[c(RGDfk)-c(GX1)] 1 h after injection (33 MBq/0.1 mL); *arrows* indicate different parts of the animal's head. Nissl staining of rats brain with intracranial glioma **b** 4× objective visualization of striatum tumor; **c** naked eye visualization of striatum tumor; **d** 4× objective visualization of cortex tumor; **e** naked eye visualization cortex tumor

situations, but achieved the best result at 1 h with U87MG cells.

Total entries and distance traveled are the classical parameters for evaluation of animal motor activity (Campos et al. 2013). The glioblastomas of these animals were limited to primary and secondary cortex areas (M1 and M2), and motor losses are described in the literature after damage in those areas (Carmel and Martin 2014; Hou et al. 2006). Also the involvement of striatum nucleus leads to motor deficit (Wang et al. 2014), however, animals didn't present such deficit, probably due to limited tumor size.

Rearing is considered an exploratory and investigatory behavior, which is normally increased in anxiety situations, as occurs in cancer patients (Beekers et al. 2014). The open field test showed an increase in the frequency and in the time spent in this behavior, especially in the striatum tumor group. However, it is important to point out that the number of animals in this study was small.

Preclinical studies were conducted with subcutaneous tumors, a nonanatomical site for human tumors. Although technically complicated, orthotopically grown cancers present advantages, and more accurately predict the response of human tumors (Fei et al. 2010; Carmeliet and Jain 2000). Histological assessment actually confirmed tumor development in the stereotaxically injection model, with location in the animal central nervous system. The varied distribution of the tumors was probably due to cell spreading during needle withdrawal, at the end of injection. A tumor in the striatum, confirmed by histology, with the size ≥1 mm, was selected for animal SPECT/CT imaging as a proof of concept. The size of the tumor is important due to the equipment resolution (1 mm). It was possible to visualize the tumor, which indicates that SPECT imaging with $^{99m}$Tc-HYNIC-E-[c(RGDfk)-c(GX1)] can be a promising tool for tumor diagnosis.

## Conclusion

Both radiotracers showed tumor specificity, however the performance of $^{99m}$Tc-HYNIC-E-[c(RGDfk)-c(GX1)] was better than $^{99m}$Tc-HYNIC-PEG$_4$-c(GX1), probably due to the combined approach of two peptides which allows the simultaneously binding of multiple receptors presented in the glioma tissue. In this sense, it should be considered in future studies, aiming to evaluate degree of angiogenesis in gliomas as well as other tumor models.

**Acknowledgments** The authors are grateful to Ana Funari, Aryel Heitor and Daniele Seo for the assistance during some experiments.

**Compliance with ethical standards**

**Conflict of interest** The authors declare that they have no conflict of interest.

**Funding** Fundação de Amparo a Pesquisa do Estado de São Paulo, Brazil [Fapesp 2011/12405-0].

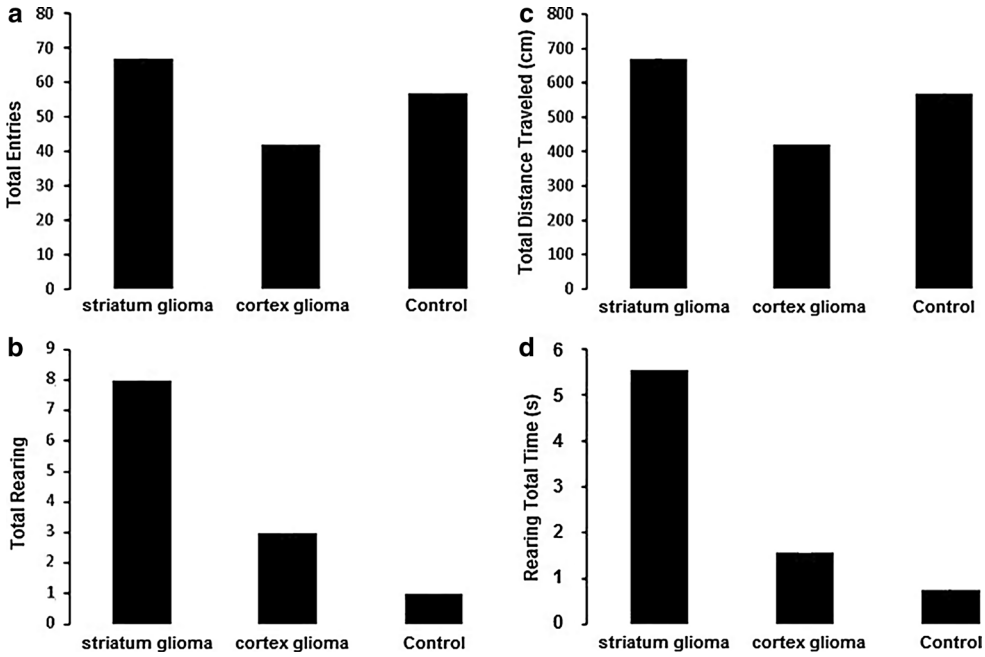


**Fig. 5** Open field test in rat model with intracranial glioma **a** total of entries; **b** total distance traveled; **c** total rearing; **d** rearing total time

**Ethical approval** All applicable international, national, and/or institutional guidelines for the care and use of animals were followed.

## References


Achilefu S (2004) Lighting up tumors with receptor-specific optical molecular probes. Technol Cancer Res Treat 3(4):393–409

Beekers N, Husson O, Mols F, van Eenbergen M, van de Poll-Franse LV (2014) Symptoms of anxiety and depression are associated with satisfaction with information provision and internet use among 3080 cancer survivors: results of the PROFILES Registry. Cancer Nurs. doi:10.1097/NCC.0000000000000184

Bello L, Giussani C, Carrabba G, Pluderi M, Costa F, Bikfalvi A (2004) Angiogenesis and invasion in gliomas. Cancer Treat Res 117:263–284

Campos AC, Fogaça MV, Aguiar DC, Guimarães FS (2013) Animal models of anxiety disorders and stress. Rev Bras Psiquiatr 35(Suppl. 2):S101–S111

Carmel JB, Martin JH (2014) Motor cortex electrical stimulation augments sprouting of the corticospinal tract and promotes recovery of motor function. Front Integr Neurosci 18:8–51

Carmeliet P, Jain RK (2000) Angiogenesis in cancer and other diseases. Nature 407(6801):249–257

Chen K, Sun X, Niu G, Ma Y, Yap LP, Hui X, Wu K, Fan D, Conti PS, Chen X (2012) Evaluation of 64Cu labeled GX1: a phage display peptide probe for PET imaging of tumor vasculature. Mol Imaging Biol 14(1):96–105

Desgrosellier JS, Cheresh DA (2010) Integrins in cancer: biological implications and therapeutic opportunities. Nat Rev Cancer 10:9–22

Durkan K, Lambrecht FY, Unak P (2007) Radiolabeling of bombesin-like peptide with 99mTc: 99mTc-litorin and biodistribution in rats. Bioconjug Chem 18:1516–1520

Fei XF, Zhang QB, Dong J, Diao Y, Wang ZM, Li RJ, Wu ZC, Wang AD, Lan Q, Zhang SM, Huang Q (2010) Development of clinically relevant orthotopic xenograft mouse model of metastatic lung cancer and glioblastoma through surgical tumor tissues injection with trocar. J Exp Clin Cancer Res 29(1):84

Gautam A, Kapoor P, Chaudhary K, Kumar R, Raghava GP (2014) Tumor homing peptides as molecular probes for cancer therapeutics, diagnostics, and theranostics. Curr Med Chem 21:2367–2391

Guo W, Giancotti FG (2004) Integrin signalling during tumour progression. Nat Rev Mol Cell Biol 5:816–826

Hou BL, Bradbury M, Peck KK, Petrovich NM, Gutin PH, Holodny AI (2006) Effect of brain tumor neovasculature defined by rCBV on BOLD fMRI activation volume in the primary motor cortex. Neuroimage 32(2):489–497

Hu H, Yin J, Wang M, Liang C, Song H, Wang J, Nie Y, Liang J, Wu K (2014) GX1 targeting delivery of rmhTNFα evaluated using multimodality imaging. Int J Pharm 461(1–2):181–191

Hua C, Zhao G, Li Y, Bie L (2014) Minichromosome maintenance (MCM) family as potential diagnostic and prognostic tumor markers for human gliomas. BMC Cancer 14(1):526

Hui X, Han Y, Liang S, Liu Z, Liu J, Hong L, Zhao L, He L, Cao S, Chen B, Yan K, Jin B, Chai N, Wang J, Wu K, Fan D (2008) Specific targeting of the vasculature of gastric cancer by a new tumor-homing peptide CGNSNPKSC. J Control Release 131:86–93

Hynes RO (1992) Integrins: versatility, modulation, and signaling in cell adhesion. Cell 69(1):11–25

Jin ZH, Furukawa T, Waki A, Akaji K, Coll JL, Saga T, Fujibayashi Y (2010) Effect of multimerization of a linear Arg-Gly-Asp peptide on integrin binding affinity and specificity. Biol Pharm Bull 33(3):370–378

Koivunen E, Wang B, Ruoslahti E (1995) Phage libraries displaying cyclic peptides with different ring sizes: ligand specificities of the RGD-directed integrins. Biotechnology (NY) 13(3):265–270

Liu Z, Wang F (2010) Dual-targeted molecular probes for cancer imaging. Curr Pharm Biotechnol 11:610–619

Okarvi SM (2004) Peptide-based radiopharmaceuticals: future tools for diagnostic imaging of cancers and other diseases. Med Res Rev 24(3):357–397

Oliveira EA, Faintuch BL (2015) Radiolabeling and biological evaluation of the GX1 and RGD-GX1 peptide sequence for angiogenesis targeting. Nucl Med Biol 42(2):123–130

Ong BY, Ranganath SH, Lee LY, Lu F, Lee HS, Sahinidis NV, Wang CH (2009) Paclitaxel delivery from PLGA foams for controlled

release in post-surgical chemotherapy against glioblastoma multiforme. Biomaterials 30:3189–3196

Ostrom QT, Gittleman H, Farah P, Ondracek A, Chen Y, Wolinsky Y, Kruchko C, Barnholtz-Sloan JS (2013) CBTRUS statistical report: primary brain and central nervous system tumors diagnosed in the United States 2006–2010. Neuro-Oncol 15(sup 2):ii1–ii56

Oyen WJG, Bodei L, Giammarile F, Maecke HR, Tennvall J, Luster M, Brans B (2007) Targeted therapy in nuclear medicine—current status and future prospects. Ann Oncol 18:1782–1792

Pasqualini R, Koivunen E, Ruoslahti E (1997) Alpha v integrins as receptors for tumor targeting by circulating ligands. Nat Biotechnol 15(6):542–546

Pasqualini R, Arap W, McDonald DM (2002) Probing the structural and molecular diversity of tumor vasculature. Trends Mol Med 8(12):563–571

Reubi JC (1997) Regulatory peptide receptors as molecular targets for cancer diagnosis and therapy. Q J Nucl Med 41:63–70

Reubi JC, Mäcke HR, Krenning EP (2005) Candidates for peptide receptor radiotherapy today and in the future. J Nucl Med 46(Suppl 1):67S–75S

Ruoslahti E, Pierschbacher MD (1986) Arg-Gly-Asp: a versatile cell recognition signal. Cell 44(4):517–518

Skobe M, Rockwel LP, Goldstein N, Vosseler S, Fusenig NE (1997) Halting angiogenesis suppresses carcinoma cell invasion. Nat Med 3:1222–1227

Song KM, Lee S, Ban C (2012) Aptamers and their biological applications. Sensors (Basel) 12(1):612–631

Strijkers GJ, Kluza E, Van Tilborg GA, van der Schaft DW, Griffioen AW, Mulder WJ, Nicolay K (2010) Paramagnetic and fluorescent liposomes for target-specific imaging and therapy of tumor angiogenesis. Angiogenesis 13(2):161–173

Ueberberg S, Schneider S (2010) Phage library-screening: a powerful approach for generation of targeting-agents specific for normal pancreatic islet-cells and islet-cell carcinoma in vivo. Regul Pept 160(1–3):1–8

Wang ES, Zhang XP, Yao HB, Wang G, Chen SW, Gao WW, Yao HJ, Sun YR, Xi CH, Ji YD (2014) Tetranectin knockout mice develop features of Parkinson disease. Cell Physiol Biochem 34(2):277–287

Wu H, Chen H, Pan D, Ma Y, Liang S, Wan Y, Fang Y (2014) Imaging integrin αvβ 3 and NRP-1 positive gliomas with a novel fluorine-18 labeled RGD-ATWLPPR heterodimeric peptide probe. Mol Imaging Biol 16(6):781–792

Zhi M, Wu KC, Dong L, Hao ZM, Deng TZ, Hong L, Liang SH, Zhao PT, Qiao TD, Wang Y, Xu X, Fan DM (2004) Characterization of a specific phage-displayed peptide binding to vasculature of human gastric cancer. Cancer Biol Ther 3:1232–1235